International Gas Union Research Conference 2011

Pierre Bérest

FRANCE

TABLE OF CONTENTS

THERMOMECHANICAL ASPECTS OF HIGH FREQUENCY CYCLING IN SALT STORAGE CAVERNS

Pierre Bérest (Ecole Polytechnique, France), Benoit Brouard (Brouard Consulting, France),
Mehdi Karimi-Jafari (Geostock) and Cyril Pelizzaro (Storengy)

Abstract

Storage of natural gas in salt caverns had been developed mainly for seasonal storage, resulting in a small number of yearly pressure cycles and moderate gas-production rates. The needs of energy traders are changing toward more aggressive operational modes.

The "high-frequency cycling" operation of salt caverns raises questions concerning the effects of frequently repeated and extreme mechanical and thermal loading. These questions concern the constitutive creep laws for salt, laboratory test procedures, criteria to be used at the design stage to provide operability, and the long-term integrity of the underground salt caverns.

Introduction

This paper focuses on the safety of deep underground salt caverns used to store natural gas or compressed air. By “deep”, we mean caverns with depths ranging between 500 and 2000 m. These caverns have been leached out from salt formations: a (typical) 1-km-deep well is cased and cemented to the rock formation, and the casing-shoe is anchored to the upper part of the salt formation. A central string is set inside the well, like a straw in a bottle, allowing soft water to be injected at the bottom of the cavern. Water leaches the salt wall, and brine is removed from the cavern through the annular space between the cemented casing and the central injection tube. After a year or more, a 10,000-m^3 to 1,000,000-m^3 cavern will be created (Figure 1). When solution-mining is completed, natural gas is injected in the cavern through the annular space, and brine is removed from the cavern through the tubing (debrining). When debrining is completed, the tubing often is removed. During operation, gas pressure varies between a minimum pressure of a few MPa and a maximum pressure that is proportional to cavern depth. (18 MPa is typical when the casing-shoe depth is 1000-m.)

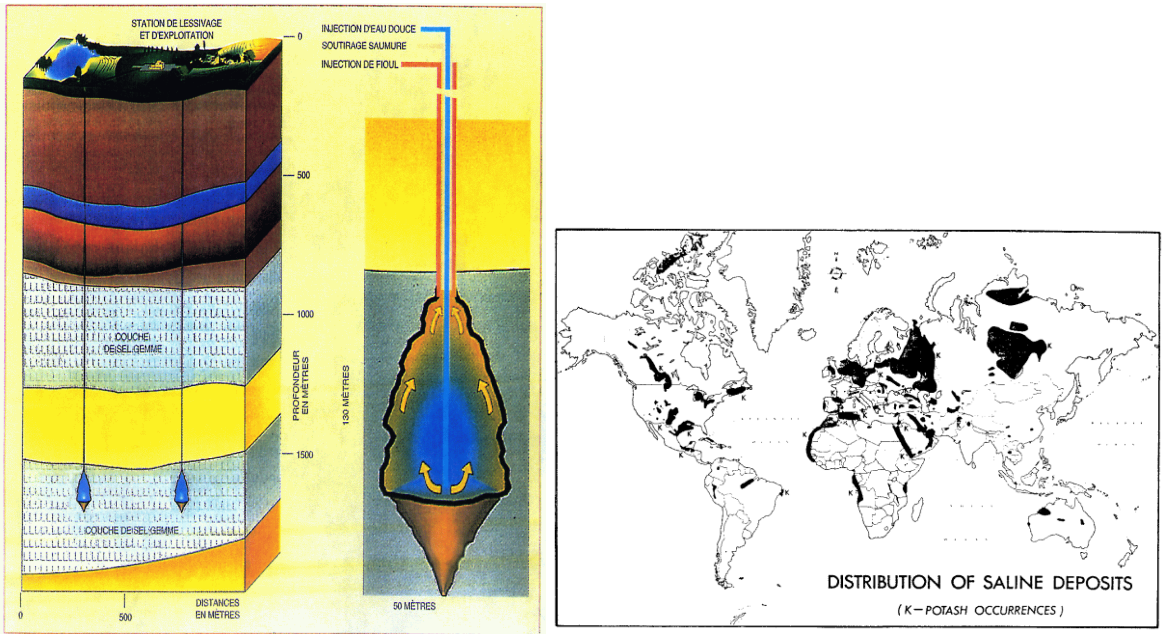

Figure 1. Leaching of a salt cavern (left) and distribution of saline deposits (Pendery, 1966).

Hundreds of such caverns have been implemented throughout the world (Thoms and Gehle, 2000); by 2010, 383 facilities were being operated in the U.S. The literature is abundant on all aspects of solution-mining techniques, including safety. The *Solution Mining Research Institute (SMRI),* which gathers companies, consultants and research centres involved in the solution-mining industry, has published hundreds of technical papers dedicated to solution-mined caverns.

Gas storage caverns were developed mainly for seasonal storage, with one or a few cycles per year and a moderate gas-production rate between the maximum and minimum operation pressure. Gas typically is injected in the summer and withdrawn in winter, when demand is higher. However, the needs of energy traders are changing toward more aggressive operating modes, with large swings to take advantage of buying and storing natural gas during low-demand periods (at low cost) to remove

and sell it during high-demand periods (at a higher price). Typically, high-deliverability caverns can be emptied in 10 days and refilled in 30 days or less (Spreckels and Crotogino, 2002).

At the same time, Compressed Air Energy Storage (CAES) is experiencing a rise in interest, as it can be used as buffer energy storage in support of intermittent sources of renewable energy such as wind mills. Off-peak periods are used to inject compressed air and to store mechanical energy. This energy is released to burn natural gas, which then is expanded in a gas turbine to generate electricity during high-demand periods. These facilities are designed to deliver their full power capacity on a very short time period. Two such facilities currently are in operation. The Huntorf facility in Germany, with a power rating of 290 MW for 2 hours, has been in operation for more than 30 years. The McIntosh facility in Alabama was commissioned in 1991; it has a power rating of 110 MW for 26 hours.

Both types of facilities (Compressed Air Energy Storage, CAES, and High-Frequency Cycled Gas-Storage Cavern, HFCGSC) imply high gas-production rate and several yearly pressure cycles. However, two differences are worth noting: (1) cycles in a CAES are more frequent than in a HFCGSC, up to one cycle per day; and (2) the gap between maximum and minimum pressure is smaller. (The Huntorf and McIntosh facilities are operated between 7 and 5 MPa.)

This cycled mode of operation of solution-mined caverns raises questions regarding frequently repeated, extreme mechanical and thermal loading. The standard approach used for designing classical gas storage (including salt constitutive creep laws, laboratory testing procedures, numerical computations and stability criteria) must be revised in this new context.

MAXIMUM PRESSURE RATE IN A SALT CAVERN

Cavern operators mainly are interested in the gas delivery rate, in Nm^3/hr. Typical figures are 1 to several 10^5 Nm^3/hr, and obviously depend on cavern volume and pressure level. From mechanical and thermal perspectives, however, the pressure decrease (or increase) rate is the most significant parameter. The pressure increase or decrease rate is limited by several factors, including compressor capacity, head losses in the tubes, hydrate formation at the wellhead (when gas pressure is low), erosion in the tubes, and rock mechanics issues (the main topic of this paper).

The gas-state equation can approximately be written $PV = mrT$; however, cavern volume changes are exceedingly small. On the other hand, an (extremely) rapid gas withdrawal is adiabatic:

$$\dot{P}/P = \dot{m}/m + \dot{T}/T \qquad \dot{T}/T = (1 - 1/\gamma)\,\dot{P}/P \quad \text{and} \quad \dot{P}/P = \gamma\,\dot{m}/m \tag{1}$$

When cavern pressure is $P = 20$ MPa, a withdrawal rate of $\dot{m}/m = 5\%/\text{day}$ generates a pressure-drop rate of $\dot{P} = 1.4$ MPa/day and a temperature-drop rate of $\dot{T} = 6$ °C/day. (In fact, it will be proved that temperature changes are smaller, because of heat transfer to the rock mass.) Typical pressure rates in seasonal storages are 0.8-1 MPa/day. (Gilhaus (2007) suggests 1-2 MPa/day.) In CAES, pressure-drop rates are faster [0.5 MPa/hr is typical at Huntorf (Crotogino et al., 2001).] and maximum pressure rates can be as fast as 1.5 MPa/hr.

Such fast pressure- and temperature-drop rates raise the issue of cavern wall stability. Field evidence is not very helpful in this context. On one hand, most gas-storage caverns were designed correctly, and very few rock-mechanics incidents are reported. (Some caverns with a depth deeper than 1500 m experienced fast creep-closure rates, up to several % per year, but they remained stable.) On the other hand, precise *in situ* measurements are difficult: damage cannot be observed at real time; and sonar surveys are able to measure cavern shape, although their accuracy normally is only 2-5%, which is too large to detect small shape evolutions. Intense salt slabbing at the cavern wall in principle should lead to a rise of the cavern bottom, a move that often is easily detectable, as it generates a rise of the brine-gas interface (when brine tubing was left after debrining). Significant bottom rises sometimes are , but their interpretation is not easy, as they can be due to slabs falling to the cavern bottom (not changing the volume occupied by gas), to cavern creep closure (indeed changing the volume occupied by gas), or to a combination of both; discrimination is difficult. Cole (2002) describes the two Markham caverns in Texas whose working gas volume is cycled 8 to 10 times each calendar year (pressure rates not mentioned). The top of the caverns top is at a depth of 1000 m. Ten years after cavern creation, losses of storage volume were observed: the bottom of cavern 2, whose initial height was 520 m, had risen by 9 m; for cavern 5, the figures were 680 m and 12 m. However, it is difficult to say whether these relatively large deformations must be attributed to cycling or to low gas pressures. Crotogino et al. (2001) report more than 20 years of operation at the Huntorf CAES facility, which includes two 750-m deep caverns. Sonar surveys were difficult to run because of humidity in the compressed air. A sonar using laser, performed in 2001 when cavern pressure was lowered to zero, proved “practically no deviation compared to the previous sonar performed in 1984 (Crotogino et al., p.356)”.

CAVERN THERMODYNAMICS

Gas temperature

Rock mass temperature increases with depth. A typical value of the geothermal gradient in a salt formation is $G = 1.6\times10^{-2}$ °C/m: in a 400-m high cavern, the salt temperature is warmer at the bottom of the cavern than at the top of the cavern by 6.4 °C or so. However, when cavern gas has been kept idle for a couple of days, gas temperature is almost uniform throughout the cavern. In fact, gas is slightly warmer and less dense at the bottom of the cavern. Due to gravity forces, it swiftly moves upward and is replaced by colder gas flowing down from the top of the cavern. Gas flow clearly is turbulent (Kneer et al., 2002). Gas is stirred by thermal convection and, as a result, gas temperature gradients are quite small (Figure 2).

When cavern pressure increases (during gas injection) or decreases (during gas withdrawal), gas temperature increases or decreases accordingly. Thermal convection is still active, and temperature gradients remain small (Figure 3).

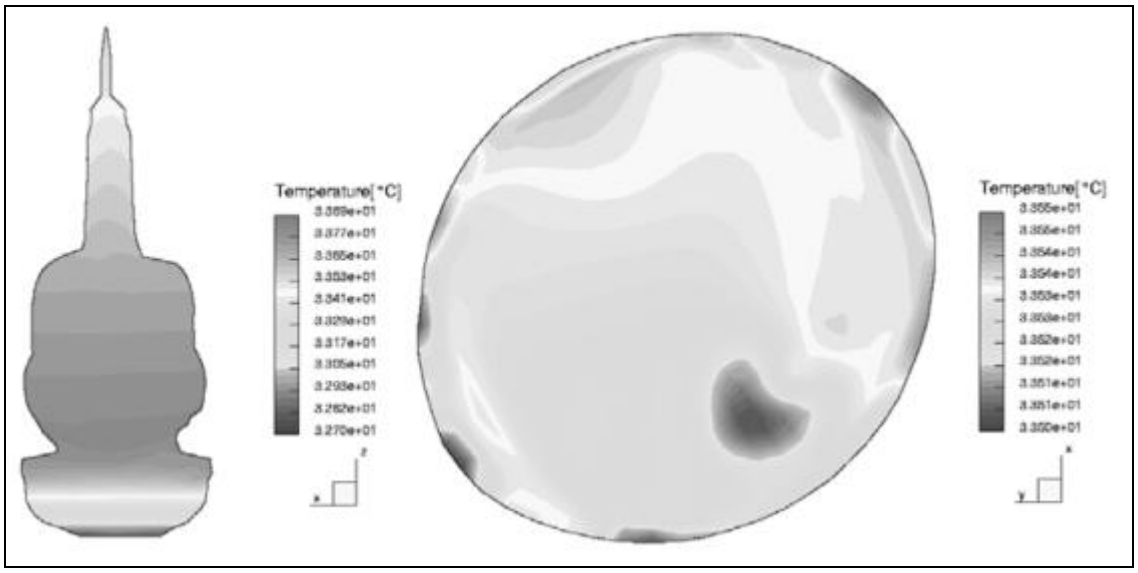

Figure 2. Computed temperature distribution in a vertical and horizontal cross-sections of a gas cavern. Note that in the horizontal section, temperature differences are smaller than 0.05°C (Klafki et al., 2003).

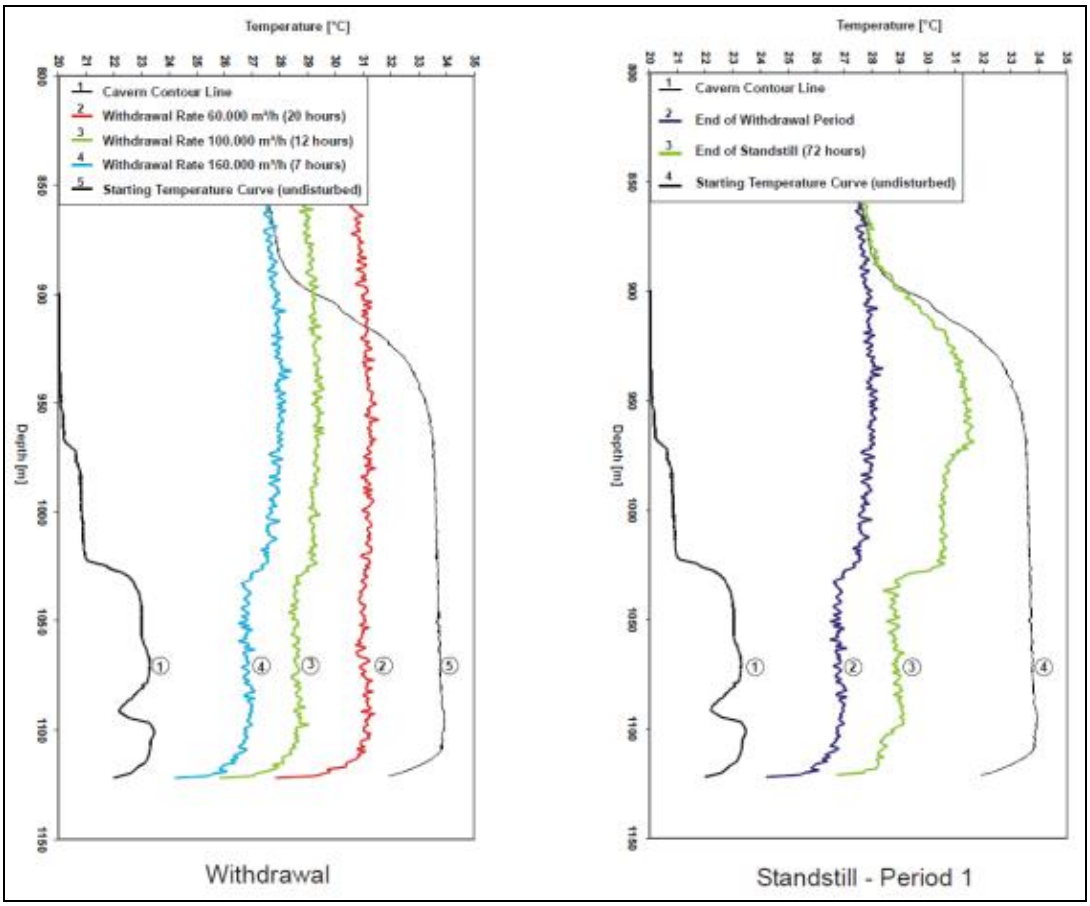

Figure 3. Shown are cavern profile (1), on the left-hand side of the two pictures (Cavern depth is 968-1070 m.), and three withdrawal tests were performed: (2) 60,000 m^3/hr for 20 hours; (3) 100,000 m^3/hr for 12 hours; and (4) 140,000 m^3/hr for 7 hours. The initial gas temperature is 34°C. (The temperature drop is 3°C, 5°C, 7°C, for the three withdrawal tests, respectively.) Note the small gas-temperature gradient, the effect of cavern diameter and the effect of the brine sump at cavern bottom (Klafki et al., 2003).

This is not exactly true when some brine is left at the bottom of the cavern after debrining. Convection also takes place in the brine at the bottom of the cavern; in addition, cavern gas is saturated with vapour and, when temperature and pressure change, condensation or vaporization takes place at the brine/gas interface, resulting in a complicated thermal balance in the vicinity of the interface, and the cavern bottom often is colder than the rest of the cavern.

Energy balance equation

When it is assumed that gas temperature T and pressure P are almost uniform in the entire cavern, the heat balance equation can be written (ATG, 1986):

$$m\left(C_p\dot{T}+\frac{1}{\rho^2}T\left.\frac{\partial\rho}{\partial T}\right|_P\dot{P}\right)=\int_{\partial\Omega}-K\frac{\partial T_{salt}}{\partial n}da+\dot{m}C_p\left(T_{inj}-T\right) \tag{2}$$

where ρ, m, V are gas density, mass and volume, respectively. Kinetic energy is neglected. The left-hand side reflects the internal energy changes minus the work of the external forces; C_P is the constant-pressure specific heat of the gas. The right-hand side is the sum of the heat flux crossing the cavern walls plus the enthalpy flux that enters the cavern during gas injection, $\dot{m}>0;\ T_{inj}$ is the temperature of the injected gas. This flux vanishes when no gas is injected in the cavern, $\dot{m}\le 0$. (The heat flux term will be discussed later.) The gas-state equation can be written $P=\rho rTZ(P,T)$, where $Z(P,T)$ is the gas compressibility factor, which can be significantly less than 1 for a natural gas. For simplicity, however, $Z=1$ is accepted in the following. By definition, $m=\rho V$; however, the cavern-creep closure rate is relatively slow, and, during rapid pressure changes, cavern volume changes are mainly elastic and exceedingly small (typically, $[dV/dP]/V=10^{-4}$ /MPa); $m=\rho V_0$ can be accepted.

The adiabatic assumption

We consider first the case of a single pressure cycle: initial cavern pressure and temperature are P_M and T_M, respectively, decreasing to P_m and T_m. Pressure then increases back to P_M, and the final temperature is T'_m. We assume first that cycles are fast and that the heat flux from the rock mass can be neglected. During a withdrawal phase, $\dot{m}<0,$ the energy balance equation and state equation can be written

$$m\left(C_p\dot{T}-\dot{P}/\rho\right)=0\qquad\text{and}\qquad\dot{P}/P=\dot{m}/m+\dot{T}/T \tag{3}$$

From these, the classical adiabatic relation can be inferred:

$$T_m/T_M=\left(P_m/P_M\right)^{1-\frac{1}{\gamma}} \tag{4}$$

Conversely, during a withdrawal phase, the heat equation must be written

$$m\left(C_p\dot{T}-\dot{P}/\rho\right)=\dot{m}C_p\left(T_{inj}-T\right) \tag{5}$$

from which it can be inferred that

$$\frac{P_M}{P_m}=\frac{\gamma T_{inj}/T_m-1}{\gamma T_{inj}/T_M^{'}-1} \tag{6}$$

From (4), it can be inferred that gas temperature is much colder at the end of the withdrawal phase than at the beginning; from (6), it can be inferred that, when the injection temperature is high, the maximum gas temperature is warmer at the end of a cycle than it is at the beginning of the cycle. However, temperatures changes computed using the adiabatic assumption are too large: in an actual cavern, even rapid temperature changes lead to large transient heat transfer from the rock mass.

Heat conduction in the rock mass

Heat conduction in the salt mass can be described by Fourier equation:

$$\frac{\partial T_{salt}}{\partial t} = k \Delta T_{salt} \qquad T = T_{salt} \text{ at cavern wall} \qquad T_{salt} = T_{\infty} \text{ at a large distance from the cavern} \tag{7}$$

where $k = K / \rho_{salt} C_{salt}$ is the thermal diffusivity of rock salt, and $k = 3 \times 10^{-6}$ m^2/s and $K = 6$ W/m/°C are typical. T_{∞} is the geothermal temperature at cavern depth. A second boundary condition at the cavern wall is provided by equation (2).

As we are mainly interested in orders of magnitude, we can consider the case of a spherical cavern, radius a, and the simplified equation that holds when no gas is injected or withdrawn from the cavern:

$$\frac{4}{3} \pi a^3 \rho C_p \dot{T} = -4 \pi a^2 K \left. \frac{\partial T_{salt}}{\partial n} \right|_{r=a} \tag{8}$$

From dimensional analysis, two characteristic times can be inferred:

$$t_c = a^2 / k\pi \qquad t_c' = \left(\rho_{salt} C_{salt} / \rho C_p \right) \pi t_c / 3 \tag{9}$$

For instance, when $V = 64{,}000$ m^3,
$a = 25$ m, $k = 100$ m^2/yr, and $t_c = 2$ years;

$\rho C_p = 50$ kJ/m^3/°C when gas pressure is $P = 5$ MPa, $\rho_{salt} C_{salt} = 2 \times 10^6$ J/m^3/°C and

$t_c' = 0.05$ year (18 days);

t_c and t_c' are the time after which temperature perturbations in the rock mass and temperature perturbations in the fluid-filled cavern, respectively, are reduced significantly.

Steady-state heat flux is small: for instance, in a spherical cavern, it is $4\pi a^2 K (T_{\infty} - T) / a$, and generates a relatively slow temperature increase rate $\dot{T} = 3(T_{\infty} - T) / \pi t_c'$. However, *immediately* following a rapid pressure drop, gas temperature changes are much faster. Assume, for instance, that the gas temperature abruptly cools by $\delta T_0 < 0$; an intense transient heat flux takes place; when short periods of time are considered, $t_c << t_c'$, temperature evolution can approximately be described as $\delta T(t) - \delta T_0 \approx -\delta T_0 \sqrt{t_c t} / 2 t_c'$. For instance, after t = 1 hour, the initial gas-temperature change is reduced by 12%. From this simplistic computation, it can be inferred that, during a pressure drop lasting several hours, gas temperature changes are considerably lessened by heat transfer from the

rock mass and are much smaller than what could be anticipated from the adiabatic assumption. Note that in a brine-filled cavern, $t_c' \approx t_c$ and rapid pressure changes are almost perfectly adiabatic.

This clearly is confirmed by field data. For instance, Crotogino et al. (2001) mention that when emptying the air-filled Huntorf cavern from 7 MPa to 2 MPa in 16 hours, temperature decreased from 40°C to 12°C (instead of -54°C, when the adiabatic assumption is made!) during the first 12 hours.

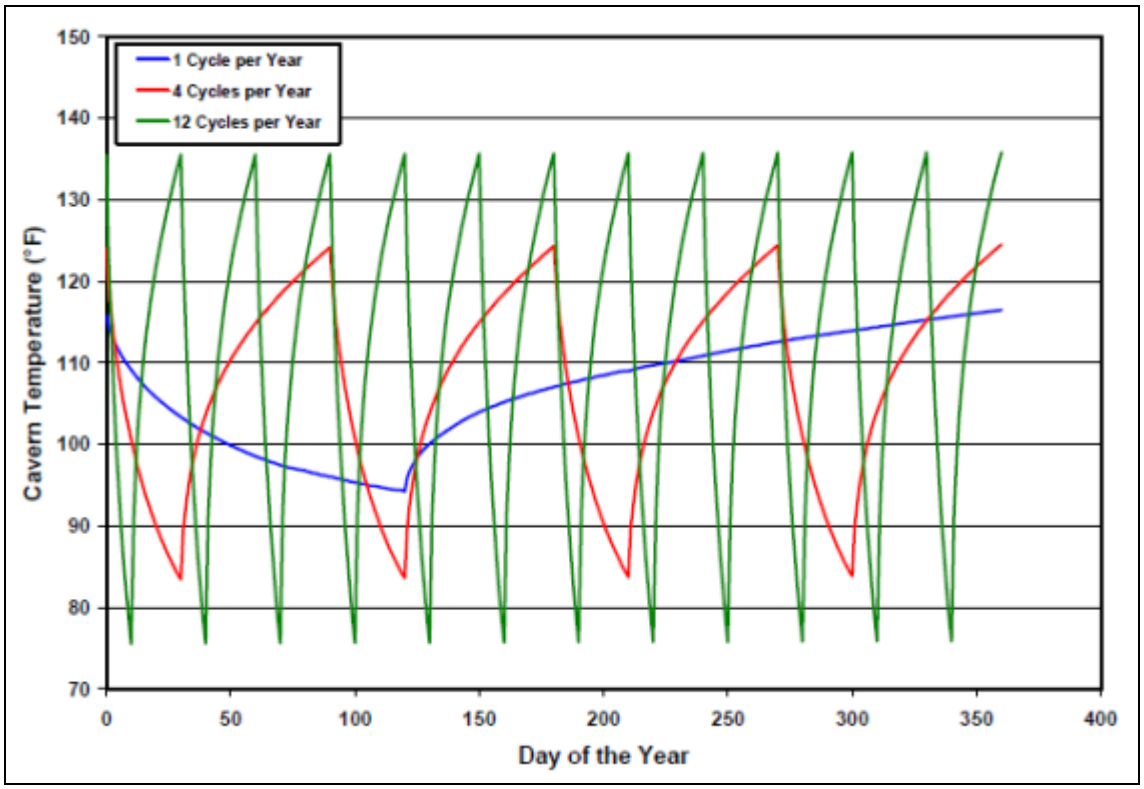

Figure 4. Natural gas temperature for a various number of cycles per year (Nieland, 2008).

Nieland (2008) computed temperature evolution in a gas-filled cavern (Figure 4) submitted to pressure cycles. Three cycle periods are considered: 1 month, 3 months and one year. The cavern volume is 160,000 m^3; the cavern top and cavern bottom are 914 m and 1219 m, respectively. Gas pressure varies between 6.0 MPa and 17.0 MPa. The gas-injection temperature (at the wellhead) is 37.8°C (100°F). Temperature fluctuations clearly are smaller when the cycle period is longer, highlighting the effect of heat transfer from the rock mass.

Depth of penetration of temperature changes

When the gas temperature cools (or warms), the rock temperature at the cavern wall also decreases (or increases). However, the depth of penetration of the temperature changes is small. A simple rule of thumb is the following: when a colder gas temperature is applied at the cavern wall and kept constant during a period δt long, the thickness of the zone at the cavern wall inside which temperature changes are not negligible is

$$\delta l = \sqrt{k \delta t / \pi} \tag{10}$$

For instance, $k = 3 \times 10^{-6}$ m^2/s, $\delta t = 2.5 \times 10^4$ s (7 hours), and $\delta l = 15$ cm. Assume that a cavern experiences a 7-hr-long pressure drop. Temperature changes only will be significant in a very small domain at the cavern wall. If the cavern is kept idle after the pressure drop, the gas temperature will increase relatively rapidly, and the "cold" domain will not be given enough time to develop.

Temperature change is a "skin effect" that only affects a thin zone at the cavern wall, but its consequences from the perspective of rock mechanics are significant.

THE MECHANICAL BEHAVIOR OF SALT AND SALT CAVERNS

The mechanical constitutive equation of salt

The mechanical behaviour of salt exhibits a fascinating complexity. It is a topic that has fostered hundreds of papers — witness the 7 Conferences dedicated to the mechanical behaviour of salt. Motivated by the needs of salt mining, hydrocarbon storage and, above all, nuclear waste disposal, no other rock has given rise to such a comprehensive set of laboratory experiments.

Most authors agree on the following. The overall strain rate, $\dot{\varepsilon}$, of a sample submitted after time $t = 0$ to a constant load, σ, is the sum of thermo-elastic, transient and steady-state parts.

The thermo-elastic part can be described by a linear relation, or $\dot{\varepsilon} = \dot{\sigma}/E + \alpha \dot{T}_{salt}$. Thermoelastic strains, or $\dot{\varepsilon} = \alpha \dot{T}_{salt}$, play an important role, as the coefficient of thermal expansion of salt, or $\alpha = 4 \times 10^{-5}/°\mathrm{C}$, is especially large for rock salt.

The transient part describes rock behaviour before steady state is reached. Any change in applied loading triggers transient creep. A stress drop triggers transient reverse creep, or $\dot{\varepsilon} < 0$ (Figure 5).

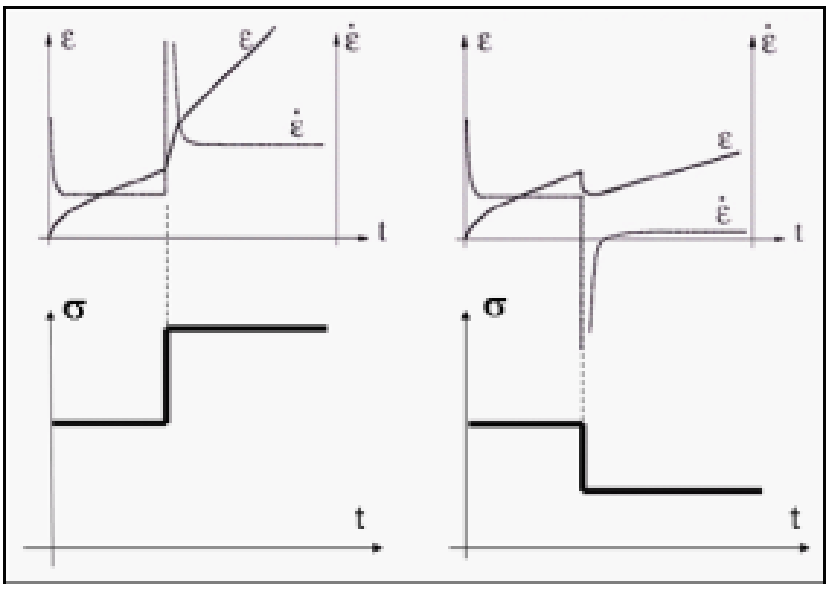

Figure 5 – Strain and strain rate as functions of time during a creep test.

The steady-state part is characterized by a constant strain rate reached after some days or weeks when a constant mechanical load is applied. Many authors agree that within the window of variations for the pressures and temperatures of interest (20 °C to 100 °C, and 0 to 30 MPa), the steady-state behaviour of salt can be described accurately by a Norton-Hoff power law, or $\dot{\varepsilon} = A\sigma^n$. The exponent of the power law is in the 3-5 range. This means that rock salt behaves as a viscous non-Newtonian fluid: any deviation from a perfectly isotropic state of stress generates salt deformation, and the strain rate is a non-linear function of the applied shear stress (more precisely, a non-linear function of the second invariant of the deviatoric stress tensor). A complete 3D formulation can be written:

$$\dot{\varepsilon}_{ij} = \frac{1+\nu}{E}\dot{\sigma}_{ij} - \frac{\nu}{E}\dot{\sigma}_{kk}\delta_{ij} + \alpha\dot{T}\delta_{ij} + \dot{\varepsilon}_{ij}^{tr} + \frac{3}{2}A\exp\left(-\frac{Q}{RT}\right)\left(\sqrt{3J_2}\right)^{n-1}s_{ij} \tag{11}$$

This formulation was fitted against the results of laboratory experiments. (A compilation for salts from a dozen different sites can be found in Brouard and Bérest, 1998.)

The mechanical behaviour of a salt cavern exhibits the same general features as the mechanical behaviour of a salt sample when, instead of the applied stress σ, one considers the difference between the geostatic pressure and the cavern gas pressure, or $P_\infty - P$, and, instead of the axial strain rate, $\dot{\varepsilon}$, one considers the cavern closure rate, or $\dot{V}/V$. When a constant pressure is applied in a cavern, the state of stresses slowly converge to a steady-state distribution characterized by a constant cavern closure rate:

$$\dot{V}/V = -A\exp\left(-\frac{Q}{RT}\right)\left(\frac{3}{2n}\right)^n\left(P_\infty - P\right)^n \tag{12}$$

In particular, the average deviatoric stress (which measures the intensity of the shear stresses) slowly decreases with time to reach its steady-state value.

State of stresses in the rock mass

Evaluation of the state of stresses in the rock mass is a difficult task for several reasons

- The state of stress is described by the six independent components of the stress tensor.
- The state of stress is a function of time. This is especially true in the case of highly cycled salt caverns, as salt mechanical behaviour is viscoplastic, and both mechanical and thermal loadings rapidly vary.
- The state of stress is a function of space. It strongly depends on the considered point inside the rock mass. When cavern shape is regular (cylindrical or spherical shape), the state of stress is somewhat similar whatever point is considered at cavern wall (slightly depending on depth). However the state of stress takes specific values in such areas as a flat roof or a non-convex part of the cavern. Generally speaking, far from the cavern walls into the rock mass, the deviatoric stress decreases, and the state of stress tends to become equal to the geostatic stress (the state of stress that prevailed before the cavern was created). Thermal stresses (i.e., additional stresses generated by a rapid change in gas temperature) are only significant inside a very thin domain close to the cavern wall.

Failure criteria

The state of stresses (or strain rates) must be compared to stability criteria. Several criteria are currently used in the literature.

❖ ***Cavern creep closure rate and subsidence rate***

Creep closure rate (in %/year) must remain slow.

❖ ***Dilation criterion***

The dilation criterion is especially important. When a varying state of stress is applied to a sample, the onset of dilatancy can be observed when shear stresses are large enough: when the sample volume strain rate becomes positive, a clear sign of the development of multiple microfractures. Dilation generally is accompanied by a loss of material strength, an increase in permeability and acoustic emission. Dilation does not mean failure; it is believed that, to some extent, a dilated material can "heal" and restore its initial strength. However, dilation can be considered a precursor of failure and, as such, the dilation criterion currently is used for dimensioning salt caverns and salt mines. The onset of a "dilated" zone must not be prohibited strictly, but the dilated zone must remain small enough (DeVries, 2006). For instance, in the case of a room-and pillar salt mine, some dilation is accepted provided that the core of the pillar remains un-dilated. The dilation criterion often is described by using two of the main invariants of the stress tensor: the mean stress, or $I_1 = (\sigma_1 + \sigma_2 + \sigma_3)/3$; and the deviatoric stress, or $J_2 = \left[(\sigma_1 - \sigma_2)^2 + (\sigma_2 - \sigma_3)^2 + (\sigma_3 - \sigma_1)^2\right]/6$ (Figure 6). Simple criteria were proposed by Spiers et al. (1988) and Ratigan et al. (1991), who suggest $\sqrt{J_2} < -0.27 I_1$ for Gulf Coast salts. More advanced formulations can be found in the literature (see, for instance, DeVries et al., 2000).

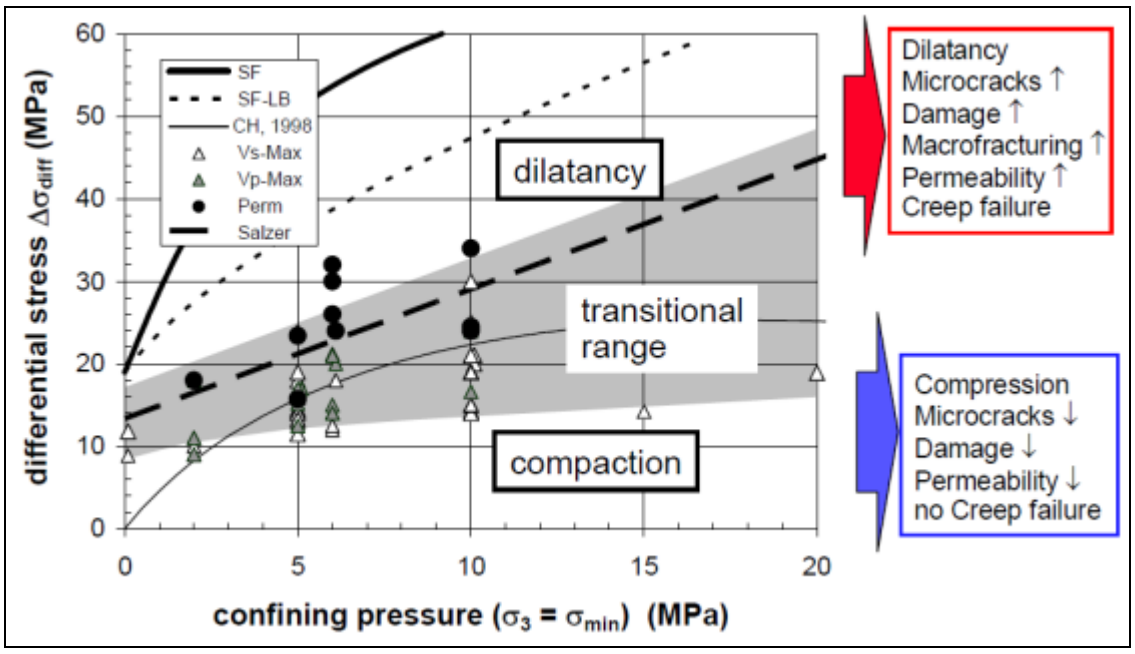

Figure 6. Dilation criterion in the $\sigma_2 = \sigma_3$, $\sigma_1 - \sigma_3$ plane (Popp et al., 2007).

There is strong evidence that the dilation criterion must be modified when, instead of a single monotonous loading, dozens of cycles are applied to the sample. For instance, Bauer et al. (2010)

cycled salt specimens from 25-30% of the dilation strength to 50-60% of the dilation strength with pauses of about 3 hours when minimum or maximum loading was reached — a loading history that mimics the kind of loading experienced in a CAES cavern. Tests were 12- to 40-days long. Dilation was observed after a certain number of cycles even if the maximum applied stress was significantly below the "static" dilation strength (i.e., as observed when monotonous loading is applied). Arnold et al. (2011) applied more frequent cycles (up to 5000 cycles) to salt samples with somewhat paradoxical results (work-hardening sometimes observed).

It must be noted that the existing dilation criteria do not depend on the stress *rate*, a possible flaw when rapid stress changes are discussed. For instance, Wallner (1984), based on a large database, stated that "the strength besides the well-known dependence on the stress also depends on the strain rate" (p.745), a concept that should be revised in the new context of rapid pressure changes in salt caverns.

❖ ***No tensile stress***

It is known that most rocks exhibit poor tensile strength. In a cavern operated according to the seasonal method, tensile stresses may appear when gas pressure is low — most often at some specific locations such as "non-convex" parts or a flat roof (Rokahr and Staudtmeister, 1996). Concerns raised by tensile stresses are more acute when high-amplitude cycles are permitted: rapid gas-pressure drops generate gas cooling and tensile "thermal stresses" at the cavern wall. When such stresses occur, , a fracture may develop. For this reason, a "no tensile stress" criterion generally is accepted when designing underground openings. One key action is to assess the extension of the fractured zone in the rock mass. When a deep fracture develops, especially at the cavern top, there is a risk of tightness loss and gas leakage to the overburden. It will be seen, however, that the zone at the cavern wall where tensile stresses are generated often is quite thin, and the risk of development of a deep fracture is likely to be small.

❖ ***No-tensile effective stress***

This criterion was first introduced by Brouard et al. (2007) and is based on observations made during hydraulic or pneumatic frac tests (performed in drill holes to assess salt mass tightness). When gas –or brine- pressure is larger than the minimum compressive stress at the cavern wall, there is a risk that a fracture may develop (Popp et al., 2007). Such a fracture may propagate — especially at the cavern roof, as full fluid pressure applies at the tip of the fracture and allows it to advance farther. Tensile effective stresses develop in two circumstances: (1) in a liquid-filled cavern after a rapid pressure increase following a long period of time during which the cavern was kept idle; and (2) in a gas-filled cavern after a rapid pressure decrease, as proved by computations recently published in the literature (Dresen and Lux, 2011; Staudtmeister and Zapf, 2010).

GEOMECHANICAL ANALYSIS

A simplified analysis

Stress computations should be performed using finite-element codes, but simplified closed-form computations provide some insight on stress evolution in the vicinity of a salt cavern. Consider, first,

the case of a spherical cavern, radius $a = 50$ m, in which gas is submitted to a daily periodic temperature evolution. After some time, steady-state stress develops in the vicinity of the cavern.

Tangential thermal stresses during a half-cycle (12 hours) are represented every 2 hours on Figure 7. The maximum intensity of the tangential stresses is $\Sigma(r) = E\alpha\delta T(r)/(1-\nu)$. Tangential stresses are large, but they vanish at a distance equal to 2% (1 m) of the cavern radius.

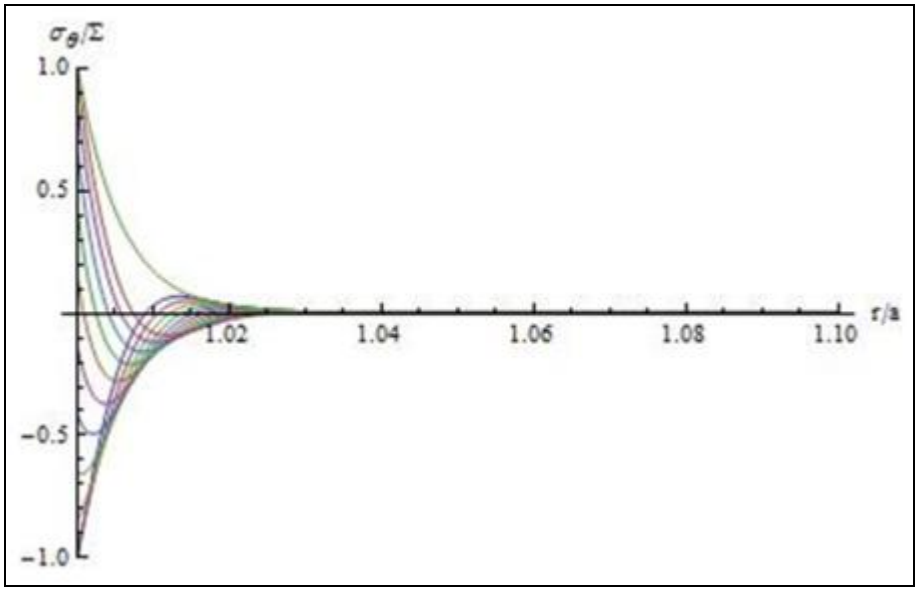

Figure 7. Tangential thermal stress distributions at the wall of an idealized spherical cavern submitted to daily pressure variations (Lestringant et al., 2010).

A second example is provided by an idealized cylindrical cavern with radius *a*. The mechanical behaviour of the salt is described by Norton-Hoff's law, in which P_∞ is the overburden pressure, and *P* is the gas pressure. It is assumed that gas pressure has been kept constant over a very long period of time. Steady-state stress distribution in the rock mass has been reached when:

$$\begin{cases} \sigma_{rr}^{ss}(r) = -P_\infty + (P_\infty - P)\left(\dfrac{a}{r}\right)^{2/n} \\ \sigma_{\theta\theta}^{ss}(r) = -P_\infty + \left(1-\dfrac{2}{n}\right)(P_\infty - P)\left(\dfrac{a}{r}\right)^{2/n} \\ \sigma_{zz}^{ss}(r) = -P_\infty + \left(1-\dfrac{1}{n}\right)(P_\infty - P)\left(\dfrac{a}{r}\right)^{2/n} \end{cases} \tag{13}$$

It easily can be verified that the values of the two invariants are:

$$\begin{cases} I_1^{ss}/3 = -P_\infty + \left(1-\dfrac{1}{n}\right)(P_\infty - P)\left(\dfrac{a}{r}\right)^{2/n} \\ \sqrt{J_2^{ss}} = \dfrac{1}{n}(P_\infty - P)\left(\dfrac{a}{r}\right)^{2/n} \end{cases} \tag{14}$$

When the pressure rapidly drops by $\delta P < 0$, additional mechanical and thermal stresses are generated:

$$\begin{cases} \delta\sigma_{rr}^{el}(r) = -\delta P \left(\dfrac{a}{r}\right)^2 \\ \delta\sigma_{\theta\theta}^{el}(r) = +\delta P \left(\dfrac{a}{r}\right)^2 \\ \delta\sigma_{zz}^{el}(r) = 0 \end{cases} \qquad \begin{cases} \delta\sigma_{rr}^{th}(r) = -\left(\dfrac{a}{r}\right)^2 \int_a^r u\Sigma(u)du \\ \delta\sigma_{\theta\theta}^{th}(r) = -\delta\sigma_{rr}^{th}(r) - \Sigma(r) \\ \delta\sigma_{zz}^{th}(r) = -\Sigma(r) \end{cases} \tag{15}$$

where $\delta T(u) < 0$ is the temperature change (cooling) generated by the $\delta P < 0$ pressure drop. When assuming adiabatic conditions, , temperature and pressure at the cavern wall satisfy the following relation:

$$\left[T + \delta T(a)\right] / T = \left[(P + \delta P)/P\right]^{1-\frac{1}{\gamma}} \tag{16}$$

(However, actual temperature changes are smaller than predicted by this relation.) *E* is the elastic modulus of rock salt, *v* is its Poisson's ratio, and *α* is its thermal expansion coefficient.

Considering typical values, $\nu = 0.25,\ \alpha = 4\times10^{-5}$ /°C, $E = 18,750$ MPa, leading to $\Sigma(r)/\delta T(r) = E\alpha/(1-\nu) \approx 1$ MPa/°C.

The new invariants are

$$\begin{cases} I_1(r)/3 = -P_\infty + \left(1-\dfrac{1}{n}\right)(P_\infty - P)\left(\dfrac{a}{r}\right)^{2/n} - \dfrac{2}{3}\Sigma(r) \\ \sqrt{J_2(r)} = \sqrt{\left[\left(\dfrac{P_\infty - P}{n}\right)\left(\dfrac{a}{r}\right)^{2/n} - \delta P\left(\dfrac{a}{r}\right)^2\right]^2 + \dfrac{1}{3}\Sigma(r)^2 - \Sigma(r)\left[\left(\dfrac{P_\infty - P}{n}\right)\left(\dfrac{a}{r}\right)^{2/n} - \delta P\left(\dfrac{a}{r}\right)^2\right]} \end{cases} \tag{17}$$

Dilation criterion

In the $\left[I_1/3, \sqrt{J_2}\right]$ diagram, it appears that the effect of a rapid (adiabatic) pressure drop is to increase both the (negative) mean pressure and the deviatoric stress.

Inside the rock mass (say, at a distance of 1 m from the cavern wall), temperature changes are negligible, and the above formula can be applied provided that $\Sigma(r) = 0$ is assumed. The dilation criterion typically is reached at the cavern wall — not at a small distance from the cavern wall in the rock mass.

This closed-form solution only provides the general trend and is of limited practical interest because; viscoplastic effects cannot be taken into account. Staudtmeister and Zapf (2010) performed the same kind of analysis using the finite element method (Figure 8). They take into account heat transfer from the rock mass: temperature changes are smaller, and deviatoric stresses decrease rapidly due to the viscoplastic behaviour of the salt mass. However, general trends are the same as in the simplified computation (Figure 8). Simulation 1 does not take into account temperature changes; it approximately holds for a point located beyond a short distance from the cavern. The closed-form solution (17) predicts that the (1)-(2) path in solution 1 should be a straight vertical line.

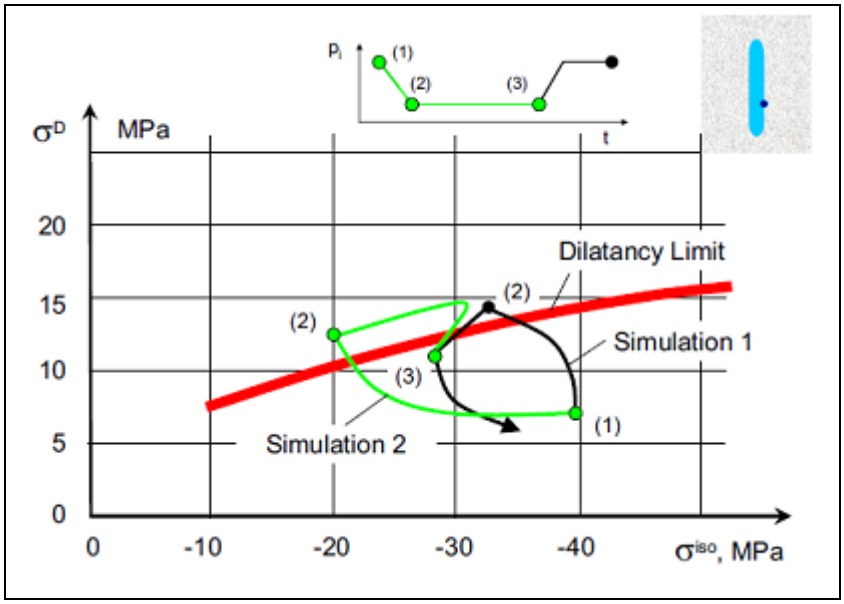

Figure 8. "Bumble Bee Flight" (Staudtmeister and Zapf, 2010). The state of stresses is calculated at the cavern wall, at the lower third of the cavern height. Cavern pressure evolution is represented in the upper figure; in the lower figure, the path followed by a point representative of the two invariants $\sigma^{iso} = I_1/3$ and $\sigma^{D} = \sqrt{2J_2}$ is represented. Simulation 2 takes into account thermal effects.

Tensile "effective" stress

Consider again the simplified model of a cylindrical cavern submitted to a rapid pressure drop. The vertical stress, or σ_{zz}, is the least compressive stress when cavern pressure is low and the vertical effective stress can be written as

$$\sigma_{zz}(r) + P + \delta P = -\frac{1}{n}(P_\infty - P) + \delta P - \Sigma(r) \tag{18}$$

During a pressure drop, δP and δT are both negative, and, in many cases, the effective stress is tensile. This also is proved by numerical computations.

Staudtmeister et al. (2011) computed the three main stresses developing at the wall of a salt cavern submitted to a couple of cycles (Figure 9). During a pressure drop, one of the two tangential stresses becomes less compressive than the normal stress at the cavern wall, and tensile effective stress develops. Similar results were found by Dresen and Lux (2011).

Tensile stresses are more difficult to reach, as a swift and large pressure drop is needed.

Multi-cycled caverns

In a multi-cycled CAES cavern, mechanical analysis is more difficult, as pathways in the invariant plane are complicated. Numerical computations are needed. An example is provided in Figure 10.

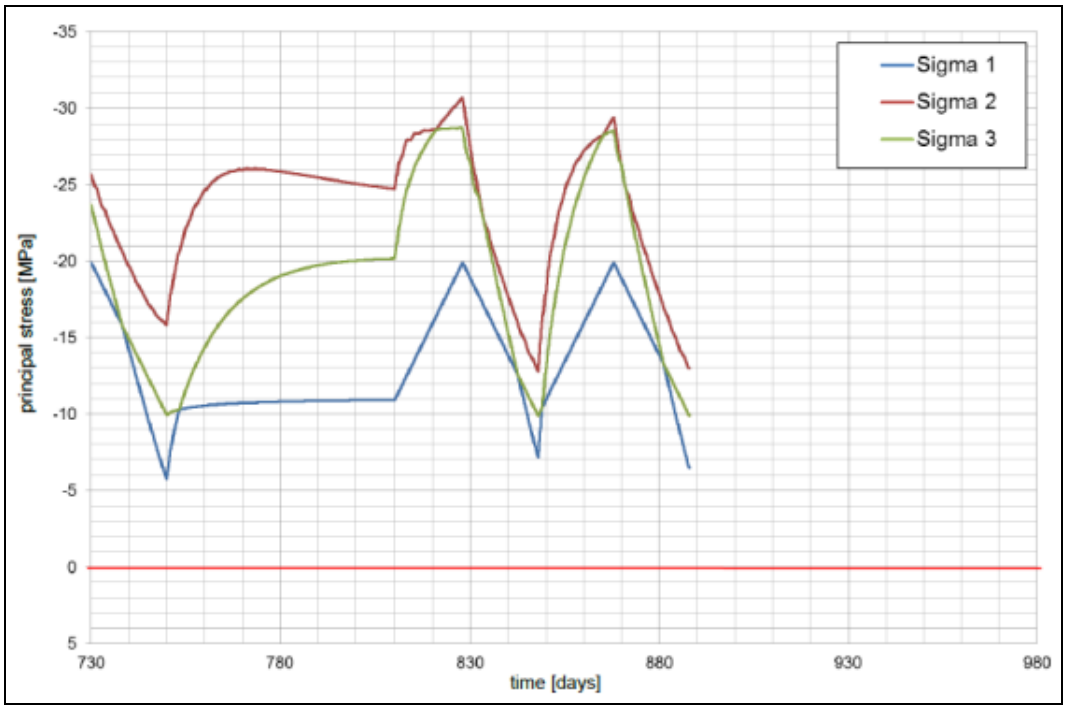

Figure 9. Main stresses at the wall of a natural gas cavern submitted to pressure cycles (Staudtmeister et al., 2011).

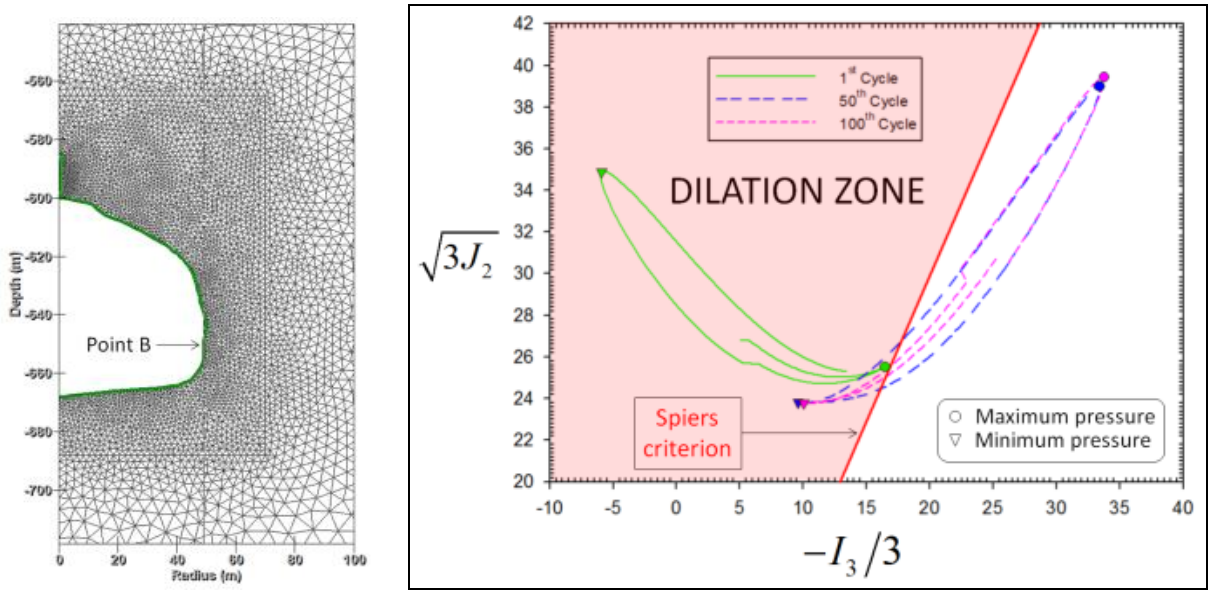

Figure 10. Cavern shape (left) and stress path in the invariants plane (right) (Brouard et al., 2011).

In this example, the cavern volume is 350,000 m^3, the casing-shoe depth is 585 m, and the cavern height is 83 m. Figure 10 displays the stress invariant pathways in the invariant plane after 1, 50 and 100 cycles. Note the slow evolution of the closed curve, which represents the pathway followed during a cycle in the invariant plane. Shear stresses are especially intense during the first cycle, and they slowly decrease with time — a general trend already observed in a cavern whose pressure remains constant.

CONCLUSIONS AND OPENED QUESTIONS

In seasonal gas storage in a salt cavern, gas pressure changes are slow, and heat transfer from the rock mass to the gas mass is allowed enough time to prevent large temperature changes associated with gas pressure to decrease or increase.

In a gas-storage cavern submitted to faster pressure changes, larger temperature changes occur. However, the adiabatic assumption is too severe; heat transfer generally is able to mitigate, at least to some extent, the temperature changes associated with rapid pressure changes. Numerical computations are needed.

Severe gas-pressure drops are a concern, as they generate severe gas cooling and large additional tensile stresses at the cavern wall. With an order of magnitude of 1 MPa/°C, they also generate dilation and effective tensile stresses. Both may lead to rock fracturing and gas leakage. The cavern roof is an especially sensitive area in this respect, although when gas is left idle after a severe temperature drop, the initial temperature is restored within a couple of days or weeks (depending on cavern size and gas pressure).

The depth of penetration of temperature changes and tensile stresses is thin (several decimetres). Furthermore, the generated fractures are perpendicular to the cavern wall and do not generate "spalls" (in sharp contrast with the effects of severe temperature increase). In the long term, repeated severe temperature changes may lead to salt spalling, but generalized collapse is unlikely.

Daily or weekly pressure cycles in a CAES storage are less severe, as the difference between maximum and minimum pressure generally is small (typically, 2 MPa). However, several studies prove that the dilation criterion to which the state of stress in the rock mass must be compared is more severe when stresses are "cycled" than when stress evolution is monotonous (as it generally is during standard laboratory tests). Whether this criterion is sensitive to stress rate is an open question. Whether the constitutive equation of salt must be modified to take into account cycling also remains open to discussion. It is a difficult problem, as it requires a large number of laboratory experiments. Field evidence is relatively scarce when rapid pressure drops are concerned, as field data often are difficult to interpret. The same can be said of CAES. However, it must be mentioned that that two CAES facilities have been operated successfully over several decades.

Acknowledgements. This study was funded partially by the French *Agence Nationale de la Recherche* in the framework of the SACRE Project, which includes researchers from EDF, Géostock, PROMES, HEI and Ecole Polytechnique.

REFERENCES

1. Pendery E.C. (1966). Distribution of salt and potash deposits; present and potential effect on potash economics and exploration. Proc. 3rd Symposium on Salt Northern Ohio Geological Society, Inc. Vol.2:85-95.

2. Thoms R.L. and Gehle R.M. (2000) A brief history of salt cavern use (keynote paper). Proc. 8th World Salt Sympsium, R.M. Geertman ed., Elsevier, **I:**207-214.

3. Spreckels H. and Crotogino F. (2002). Salt Caverns for Peak Shaving – Reservoirs for Seasonal Balance? New Market Requirements and appropriate Storage solutions. SMRI Fall Meeting, Bad Ischl, Austria, 299-313.

4. Crotogino F., Mohmeyer K.U, Scharf R. (2001). Huntorf CAES: More than 20 Years of Successful Operation. SMRI Spring Meeting, Orlando, Florida, 351-362.

5. Gilhaus A. (2007). Natural Gas Storage in salt Caverns – Present Status, Developments and Future Trends in Europe. SMRI Spring Meeting, Basel, Switzerland, 69-87.

6. Cole R. (2002). The long Term Effects of High Pressure Natural Gas Storage on Salt Caverns. SMRI Spring Meeting, Banff, Alberta, Canada, 75-97.

7. Kneer A. Irmer A., Riegel H., Klafki M. (2002). Application of a CFD-Code for Modeling of 3-D Processes in salt Caverns During Gas Withdrawal. SMRI Fall Meeting, Bad Ischl, Austria, 197-209.

8. Klafki M., Wagler T., Grosswig S., Kneer A. (2003). Long-term downhole fibre optic temperature measurements and CFD modeling for investigation of different gas operating modes. SMRI Fall Meeting, Chester, UK, 180-189.

9. ATG (1986). Stockages souterrains de gaz (Underground gas storages). Manuel pour le transport et la distribution du gaz, Titre XIII. Association technique de l'industrie du gaz en France, 62 rue de Courcelles, 75008 Paris France (in French).

10. Nieland JD. (2008). Salt cavern Thermodynamics-Comparison Between Hydrogen, Natural Gas and Air Storage. SMRI Fall Meeting, Austin, Texas, 215-234.

11. Brouard B., Bérest P. (1998). A tentative classification of salts according to their creep properties. Proc. SMRI Spring Meeting, New Orleans, Louisiana, 8-38.

12. DeVries K.L. (2006). Geomechanical Analyses to Determine the Onset of Dilation around Natural Gas Storage Caverns in Bedded Salt. Proc. SMRI Spring Meeting, Brussels, 131-150.

13. Spiers, C.J., Peach C.J., Brzesowsky R.H., Schutjens P.M., Liezenberg J.L., and Zwart H.J. (1988). Long Term Rheological and Transport Properties of Dry and Wet Salt Rocks, EUR 11848, prepared for Commission of the European Communities, by University of Utrecht, Utrecht, The Netherlands.

14. Ratigan, J. L., L. L. Van Sambeek, K. L. DeVries, and J. D. Nieland (1991). The Influence of Seal Design on the Development of the Disturbed Rock Zone in the WIPP Alcove Seal Tests, RSI-0400, prepared by RE/SPEC Inc., Rapid City, SD, for Sandia National Laboratories, Albuquerque, NM.

15. DeVries K.L., Mellegard K.D., Callahan G.D. (2000). Cavern Design Using a Salt Damage Criterion: Proof-of-Concept Research Final Report. SMRI Spring Meeting, Houston 1-18.

16. Popp T., Brückner D., Wiedemann M. (2007). The Gas Frac scenario in rock Salt – Implications from Laboratory Investigations and Field Studies. SMRI Spring Meeting, Basel, Switzerland, 287-305.

17. Bauer S., Broome S., Bronowski D. (2010). Experimental deformation of Salt in Cycling Loading. SMRI Spring Meeting, Grand Junction, Colorado, 185-196.

18. Arnold

19. Wallner M. (1984). Analysis of thermomechanical problems related to the storage of heat producing radioactive waste in rock salt. Proc. 1st Conference on the Mechanical Behavior of salt, Trans Tech Pub, Clausthal Hannover, 739-763.

20. Rokahr R. and Staudtmeister K. (1996). The assessment of the stability of a cavern field in bedded salt with the help of the new Hannover dimensioning concept. Proc. 3rd conference on the Mechanical Behavior of salt, Trans Tech Pub, Clausthal Hannover, 533-544.

21. Brouard B., Karimi-Jafari M., Bérest P. (2007). Onset of effective tensile stresses in gas storage caverns. SMRI Fall Meeting, Halifax, Canada, 119-134.

22. Dresen R. and Lux K.H.. (2011). Method for design of salt caverns with respect to high frequency cycling of storage gas. Proceedings SMRI Spring Meeting, Galveston, 66-82.

23. Staudtmeister K. and Zapf D. (2010). Rock Mechanical Design of Gas Storage Caverns for Seasonal Storage and Cyclic Operations. Proceedings SMRI Spring Meeting, Grand Junction, Colorado,197-213.

24. Lestringant C., Bérest P., Brouard B. (2010). Thermomechanical Effects in Compressed air storage (CAES). SMRI Fall Meeting, Leipzig, Germany, 29-44.

25. Staudtmeister K., Zapf D., Leuger B. (2011). The scenarios on the thermo-mechanical behavior of a gas storage cavern. Proceedings SMRI Spring Meeting, Galveston, 83-97.

26. Brouard B., Frangi A., Bérest P. (2011). Mechanical stability of a Cavern Submitted to High-Frequency Cycles. Proceedings SMRI Spring Meeting, Galveston, 99-116.

Figures Legends

Figure 1. Leaching of a salt cavern (left) and distribution of saline deposits (Pendery, 1966).

Figure 2. Computed temperature distribution in a vertical and horizontal cross sections of a gas cavern. Note that in the horizontal section, temperature differences are smaller than 0.05°C. (Klafki et al. 2003).

Figure 3. Shown are cavern profile (1), on the left-hand side of the two pictures (Cavern depth is 968-1070 m.), and three withdrawal tests were performed: (2) 60,000 m^3/hr for 20 hours; (3) 100,000 m^3/hr for 12 hours; and (4) 140,000 m^3/hr for 7 hours. The initial gas temperature is 34°C. (The temperature drop is 3°C, 5°C, 7°C, for the three withdrawal tests, respectively.) Note the small gas-

temperature gradient, the effect of cavern diameter and the effect of the brine sump at cavern bottom (Klafki et al., 2003).

Figure 4. Natural gas temperature fluctuations for a various number of cycles per year. (Nieland, 2008).

Figure 5 – Strain and strain rate as functions of time during a creep test.

Figure 6. Dilation criterion in the $\sigma_2 = \sigma_3,\ \sigma_1 - \sigma_3$ plane (Popp et al. 2007).

Figure 7. Tangential thermal stress distributions at the wall of an idealized spherical cavern submitted to daily pressure variations (Lestringant et al., 2010).

Figure 8. "Bumble Bee Flight" (Staudtmeister and Zapf, 2010). The state of stresses is calculated at the cavern wall, at the lower third of the cavern height. Cavern pressure evolution is represented in the upper figure; in the lower figure, the path followed by a point representative of the two invariants $\sigma^{iso} = I_1/3$ and $\sigma^D = \sqrt{2J_2}$ is represented. Simulation 2 takes into account thermal effects.

Figure 9. Main stresses at the wall of a natural gas cavern submitted to pressure cycles (Staudtmeister et al., 2011)

Figure 10. Cavern shape (left) and stress path in the invariants plane (right) (Brouard et al., 2011).

Figure 2. Computed temperature distribution in a vertical and horizontal cross-sections of a gas cavern. Note that in the horizontal section, temperature differences are smaller than 0.05°C (Klafki et al., 2003).